Helium isotopes in the Izu Peninsula, Japan : relation of magma and crustal activity

Ohno, Masao
Department of Environmental Changes, Faculty of Social and Cultural Studies, Kyushu University

Sumino, Hirochika
Laboratory for Earthquake Chemistry, Graduate School of Science, The University of Tokyo

Hernandez, Pedro. A
Instituto Technológico Energías Renovables (ITER)

Sato, Tsutomu
Geological Survey of Japan, AIST

他

出版情報：Journal of Volcanology and Geothermal Research. 199 (1/2), pp.118-126, 2011-01-01. Elsevier
バージョン：

(Submitted to JVGR)

Helium isotopes in the Izu Peninsula, Japan: relation of magma and crustal activity

Masao Ohno [*1], Hirochika Sumino [2], Pedro A. Hernandez [3], Tsutomu Sato [4], and Keisuke Nagao [2]

Abstract

The relation of magma and crustal activities has been studied from spatial distribution of $^{3}He/^{4}He$ ratios of gas and/or water samples over the Izu Peninsula, where significant crustal deformation associated with seismic swarm activities has been observed since 1970's. The air-corrected values of $^{3}He/^{4}He$ ratios ranged from 3.5 to 8.2 R_A, where R_A is the atmospheric $^{3}He/^{4}He$ ratio = 1.4×10^{-6}, indicating the helium is mostly of magmatic origin Among the three pressure sources proposed to explain the crustal deformation, two inflation sources beneath the inland of northeast and the mid east coast of the Izu Peninsula locate in the broad distribution of high $^{3}He/^{4}He$ ratios, which supports relation of magma to the crustal uplift. The distribution of high $^{3}He/^{4}He$ ratios around the tensile fault assumed in the area of seismic swarms appears not to evidently indicate existence of significant amount of magma below the tensile fault. Alternatively, the result suggests magma below a point several kilometers south of the tensile fault. The seismic swarms are explained either by fluid pressurization of thermal water heated by this magma or by intrusion of magma to the tensile fault moved obliquely from the deep magma reservoir.

Key Words: helium isotope, groundwater, seismic swarm, monogenetic volcano, noble gas

[1] Department of Environmental Changes, Faculty of Social and Cultural Studies, Kyushu University, Fukuoka, 819-0395 Japan

[2] Laboratory for Earthquake Chemistry, Graduate School of Science, The University of Tokyo, Tokyo, 113-0033 JAPAN

[3] Instituto Technológico Energías Renovables (ITER), 38611, Tenerife, Canary Islands, Spain

[4] Geological Survey of Japan, AIST, Tsukuba, 305-8567 Japan.

[*] Corresponding author's Email address: mohno@scs.kyushu-u.ac.jp

1. Introduction

Significant crustal deformation has been observed in the Izu Peninsula, Japan, accompanied by seismic swarms repeated intermittently since 1970's. Several pressure sources were modeled to explain the crustal deformation and magmatic activity was assumed as the cause of pressure increase, which is supported by the submarine eruption at Teisi Knoll off Ito City in July 1989, in addition to the existence of monogenetic volcanoes around this area. However, the relation of magma and the pressure sources were not clear because crustal deformation data does not have information of material composition of the source.

The $^{3}He/^{4}He$ ratios, sensitive to magmatic gas migrating upward in the crust and seeping into shallow groundwater circulation, are expected to provide information that will help to clarify how magma is related to the crustal activity. While most ^{3}He is considered to originate in deep Earth, most ^{4}He is produced by radioactive decay of U, Th and their daughter isotopes in crustal rocks (e.g., Ozima and Podosek, 2002). At stratovolcanoes, it has been observed that $^{3}He/^{4}He$ ratio decreases with distance from the eruption center of volcanoes (Sano et al., 1984; Williams et al., 1987; Marty et al., 1989; Sakamoto et al., 1992). This can be explained by progressive leaching of crustal helium with low $^{3}He/^{4}He$ ratio as an originally ^{3}He-enriched magmatic fluid migrates through local crust. In contrast, broad distribution of high $^{3}He/^{4}He$ ratios is reported at a hot spot oceanic volcanic island (Perez et al., 1996). Quite uniform and high $^{3}He/^{4}He$ ratio was observed without any relationship with the distance from the summit crater of Teide volcano in Tenerife Island. Perez et al. (1996) interpreted the uniform and high $^{3}He/^{4}He$ ratio by degassing of magmatic gases along permeable fracture/fault systems. In general, magmatic gas especially for helium migrates through fault, dyke, fissure and porous material in the crust. Many investigations on various geotectonic environments have been reported (e.g., Hoke et al., 2000; Matsumoto et al., 2003; Shimizu et al.,

2005; Dogan et al., 2006). However, the spatial distribution of $^{3}He/^{4}He$ ratios in monogenetic volcano group fields, such as the Izu Peninsula, has not been studied precisely yet.

In this paper, we present and discuss the spatial distribution of $^{3}He/^{4}He$ ratio and isotopic and elemental compositions of other noble gases (Ne, Ar, Kr, and Xe) to clarify the relation of magma and the crustal activities in the Izu Peninsula.

2. Regional setting

2.1 Geological setting and eruption history

Almost all the formations exposed in the Izu Peninsula are volcanics and their reworked deposits (Koyama and Umino, 1991). The basement formations are submarine volcanics erupted since the early Miocene, composed of basalt, andesite, and dacite. Accompanying northward collision with the Japan arc at about 1 Ma, the Izu Peninsula was uplifted and terrestrial volcanic products deposited. After the activity of polygenetic volcanoes, the activity of the monogenetic volcanoes, in and outboard of the coast line of the Izu Peninsula (Fig. 1), started about 150,000 years ago. They are explained in relation to crustal extension caused by compressional stress perpendicular to the extension azimuth due to strong mechanical coupling of the buoyant Izu-Bonin arc to Japan arc (Koyama and Umino, 1991). The latest significant eruption is estimated to have occurred at 2,700 years ago along an eruptive fissure in the center of the field (Hayakawa and Koyama, 1992; Koyama et al., 1995). The first historical eruption of this monogenetic volcano group was a submarine eruption (magma-phreatic explosion) at Teisi Knoll off Ito City on July 13, 1989 (Fig. 1). Ejecta of the eruption were small in volume and composed of highly crystalline basalt scoria, highly vesiculated pumice, and lithic material (Yamamoto et al., 1991).

103

104 *2.2. Seismic swarm activity*

105

106 Significant crustal deformation was observed in the Izu Peninsula associated
107 with seismic activities (e.g., Okada and Yamamoto, 1991; Tada and Hashimoto, 1991;
108 Tsuneishi, 1991; Okada et al., 2000; University of Tokyo, 2000). One of the
109 characteristics of the crustal deformation is the prominent uplift in the east coast in
110 contrast to subtle descending at the west coast (Fig. 2). Three isolated pressure sources
111 were assumed to explain the crustal deformation. Source A is at a depth of 10 km
112 beneath the inland of northeast Izu Peninsula that caused uplift between 1974 and 1982.
113 Hagiwara (1977) assumed increase of its gas pressure to explain the uplift and gravity
114 decrease until 1976. Source B is beneath the east coast at a depth of 10 km that explains
115 the crustal deformation after 1978 (Tada and Hashimoto, 1991). Source C is a group of
116 intrusive tensile faults in the area of seismic swarms as follows. Okada and Yamamoto
117 (1991) and Tada and Hashimoto (1991) assumed a tensile fault (C1: thick line in Fig. 2)
118 beneath Teisi Knoll to explain the crustal deformation during 1989 event. At the
119 southeast extension of this fault, Tada and Hashimoto (1991) added deeper tensile faults
120 to explain the total crustal deformation between 1978 and 1990 (C2: thin line in Fig. 2).
121 For the succeeding seismic swarm activities between 1993 and 1998, tensile faults in
122 similar directions were assumed in the area of the seismic swarms (Yamamoto et al,
123 1994; Yoshida et al, 1999; Okada et al., 2000).
124 Given that the seismic swarms are related to magma, it has been discussed
125 further how the magma causes the seismic swarms. One hypothesis is that the seismic
126 swarms are caused by intrusion of magma into the shallow crust as dikes (e.g., Ukawa
127 and Tsukahara, 1996). The other hypothesis is that seismic swarms are a result of fluid
128 pressurization heated by magma: increase of pore pressure in the rock decreases
129 effective stress and facilitates the occurrence of faulting (e.g., Tsuneishi, 1991). In the

discussion between these hypotheses, some geophysical observations have been posed that contradict to each other. Large-scale magma intrusion was doubted for the 1989 activity from gravity measurements because the density of the cavity of the tensile fault was estimated to be small (Okubo et al., 1991); similarly, highly vesiculated magma or water was suggested as the material injected into the faults for the 1997 activity (Yoshida et al., 1999). In addition, magnetic observations (Sasai and Ishikawa, 1991; Honkura et al., 1994) are contradictory to large-scale thermal demagnetization beneath the eruption site. On the other hand, Ukawa and Tsukahara (1996) claimed that pore pressure model does not explain the observed focal depth migration because the pore pressure model expects continuous active seismicity around the dike over the whole depth range. Focal depth migration of seismic swarms has been depicted on the basis of geodetic and seismic data by many authors (e.g., Cervelli et al., 2001; Morita et al., 2006).

3. Sampling and analysis

We collected 31 samples from hot springs, cold springs, and steam wells in the study area (Table 1), covering the entire Izu Peninsula (Fig. 1). To study the spatial distribution of noble gas isotopes, we avoided the possible short-term disturbance in them related to large earthquakes or seismic swarms by collecting samples in the period of quiescence of seismic swarms between 1998 and 2002. Samples were collected in 50-ml lead glass bottles with vacuum valves on both ends. At the water wells, bubbling gas was collected by a displacement method of water (G in type in Table 1). When the content of bubbling gas was too small to fill the bottle, water was collected and the gaseous component was extracted to another evacuated 50-ml lead glass bottle in laboratory (W in type in Table 1). At steam wells, a vinyl tube was placed in the well and the steam was introduced into the bottle; the bottle was cooled by water to acquire

157 enough pressure of gas to the analysis. At hot springs and cold springs, pH and electric
158 conductivity were measured with a multi-parameter pH/conductivity meter (Cyberscan
159 300, Eutec instruments).
160 Noble gas isotopic compositions were determined using three mass
161 spectrometric systems, MS-I, MS-III and MS-IV, at the Laboratory for Earthquake
162 Chemistry, University of Tokyo. Details in each mass spectrometric system and basic
163 analytical procedure are described by Sano and Wakita (1988), Aka et al. (2001) and
164 Sumino et al. (2001) for MS-I, MS-III and MS-IV, respectively. Air standards were
165 measured frequently during analysis to determine mass discrimination factors and
166 sensitivities of the mass spectrometers for all noble gases except for the helium isotope
167 ratio. The correction factor for helium isotope ratios was determined by measurements
168 of air standard in the case of MS-I and of inter-laboratory helium standard named HESJ
169 in the case of MS-III and MS-IV. Recommended $^{3}He/^{4}He$ ratio of HESJ is 20.63 ± 0.10
170 R_A (Matsuda et al., 2002), where R_A is the atmospheric $^{3}He/^{4}He$ ratio = 1.4×10^{-6}.
171 Machine bias in helium isotope ratio among the three mass spectrometers was checked
172 by Sumino et al. (2001). There were no systematic differences exceeding analytical
173 errors among $^{3}He/^{4}He$ ratios obtained with the each mass spectrometer. Since blank
174 levels of all noble gases are less than 0.1% of the amount of sample gases, blank
175 correction was not applied. Corrections of interference peaks of $^{40}Ar^{++}$ and CO_2^{++} on
176 $^{20}Ne^{+}$ and $^{22}Ne^{+}$ were applied although the corrections were not significant because the
177 amounts of background ^{40}Ar and CO_2 are negligible as compared to the sample neon.
178
179 **4. Analytical results**
180
181 Analytical results of the noble gases from Izu Peninsula samples are listed in
182 Table 2. The concentration of noble gases and their isotopic ratios are tabulated. Errors
183 related to the isotopic ratios are one standard deviation, including statistical error during

sample analysis, error in the discrimination factor and that on the recommended $^{3}He/^{4}He$ ratio of HESJ (Matsuda et al., 2002) for the helium isotope ratio. Errors on abundance are estimated to be ten percent based on reproducibility of noble gas sensitivity of the mass spectrometer during repeated air standard analyses. Since $^{4}He/^{20}Ne$ ratios of samples No. from 28 to 31 are close to that of the atmosphere, which indicate severe contamination by air component, we remove these four samples from the discussion hereafter.

The plot of $^{3}He/^{4}He$ ratios on $^{4}He/^{20}Ne$ ratios (Fig. 3) indicates most of the helium is magmatic origin with a minor contribution of crustal component. In Table 2, the air-corrected $^{3}He/^{4}He$ ratio is calculated assuming that $^{4}He/^{20}Ne$ ratio is 0.318 ($^{4}He/^{20}Ne$ ratio of air). Although $^{4}He/^{20}Ne$ of air-saturated water (ASW) varies between 0.268 (at 20°C) and 0.335 (at 100°C, caluculated after Ballentine et al., 2002), the variation in air-corrected $^{3}He/^{4}He$ ratio is not significant to affect the discussion below. With the exception of sample No. 26, the air-corrected values (range from 5.7 R_A to 8.2 R_A) are equal to or higher than the average value (5.10±1.68 R_A) in northeast Japan compiled by Hilton et al. (2002).

The relation between $^{21}Ne/^{22}Ne$ and $^{20}Ne/^{22}Ne$ ratios aligns along a mass-dependent Rayleigh fractionation line of atmospheric neon (Fig. 4). This indicates absence of mantle-derived neon in the samples, supporting the assumption in the air-correction of helium isotope ratios, in which all neon in each sample is of atmospheric origin. Further, the lower $^{20}Ne/^{22}Ne$ ratios than the atmospheric ratio is considered to be a characteristic of residual neon in water from which a part of noble gas is removed because diffusive coefficient for each isotope in water is proportional to the inverse of the square root of its atomic mass (Peeters et al., 2002). These fractionated isotope ratios are observed irrespectively of sample type (bubbling gas/water/steam), suggesting that isotopic fractionation is not occurring during atmospheric contamination near the surface, sampling or sample handling such as gas

extraction in the laboratory. Therefore, the neon isotopic fractionation would be caused by the diffusive loss in the groundwater system.

In the $^{40}Ar/^{36}Ar$ and $^{38}Ar/^{36}Ar$ ratios (Fig. 5), non-atmospheric argon is recognized although most of the argon is of atmospheric origin with or without minor mass-dependent isotopic fractionation. The fact that the degree of $^{38}Ar/^{36}Ar$ fractionation is much smaller than that observed in neon isotopes, and that there is no correlation among neon isotope ratios and $^{38}Ar/^{36}Ar$ ratios as reported by Nagao et al. (1979) and Sumino et al. (2004), imply neon and argon mass fractionation would be caused by different processes. However, it is difficult to provide further explanation for the fractionation processes at present. To determine the origin of non-atmospheric component, mantle or crustal, fractionation-corrected $^{40}Ar/^{36}Ar$ ratios are calculated using $^{38}Ar/^{36}Ar$ ratios and assuming mass-dependent fractionation (Table 1). As most of the high fractionation-corrected $^{40}Ar/^{36}Ar$ ratios accompany high air-corrected $^{3}He/^{4}He$ ratios (samples No. 4, 9, 11, 13, 16, 21 and 25), the radiogenic ^{40}Ar, which is non-atmospheric ^{40}Ar and denoted as $^{40}Ar^*$ hereafter, is suggested to be of mantle origin. Furthermore, the $^{4}He/^{40}Ar^*$ ratios of these samples (range from 0.11 to 2.5 in Table 1) support that $^{40}Ar^*$ is of mantle origin because they are close to the mantle value ($^{4}He/^{40}Ar^* = 2$, Burnard et al., 1997). While some data show lower values than the mantle value, it would result from slightly low $^{4}He/^{40}Ar^*$ ratios (0.1-10) of mantle wedge as reported for mafic phenocrysts in lavas and mantle peridotite from arc settings (Yamamoto et al., 2009) rather than volatile fractionation during magmatic degassing, which would cause larger He/Ar change (Fischer et al., 2009). The conclusion remains unchanged if we take into account the possibility that solubility-controlled fractionation during noble gas uptake into groundwater would have increased He/Ar ratio up to a factor of five at the highest (Ozima and Podosek, 2002; Ballentine et al., 2002; Peeters et al., 2002). One exception is sample No. 4, which exhibits significant enrichment in heavy noble gases, implying a sedimentary contribution in its $^{40}Ar^*$ as discussed later.

The general feature of noble gas elemental ratios compared to those of the atmospheric composition is enrichment of helium, depleted neon, and abundant krypton and xenon. The helium enrichment up to two orders of magnitude supports that helium in the samples are dominated by mantle/crustal components. On the other hand, the heavier noble gas elemental ratios than helium of most of the water and gas/steam samples are consistent with ASW composition of a temperature range of 20-100°C as shown in the relationship of *F(132)* to *F(20)* (Fig. 6), suggesting that they mostly originate in water-dissolved atmospheric gases. The relationship of *F(84)* to *F(20)* is similar to this and not shown here. There are two exceptions which show high neon abundance and depletion in krypton and xenon. These two samples (No. 17 and 25) contained about 50 vol% of water in their sample bottles. While gaseous components in the other water samples are almost completely extracted, those of the two samples were directly introduced into the noble gas purification line without extraction procedure. Therefore, the heavy noble gases which have higher solubility and lower diffusivity in water than the light noble gases (Ozima and Podosek, 2002; Ballentine et al., 2002; Peeters et al., 2002) were left in the water phase in the sample bottles before reaching equilibrium in the sample purification line. This may give rise to elemental fractionation of $^{4}He/^{20}Ne$ ratios of these samples. However, less than 20% difference in solubilities of helium and neon and their higher diffusivities do not cause significant change in $^{4}He/^{20}Ne$ ratio, while solubilities of heavy noble gases are 3-20 times larger than that of helium (Ozima and Podosek, 2002; Ballentine et al., 2002; Peeters et al., 2002). After the two gas/water samples possibly affected by artifact have been excluded, some of the gas/steam samples show significantly higher *F(132)*, *F(84)*, and/or *F(20)* than those of ASW (Table 2, Fig. 6). The enrichment in heavy noble gases compared to ASW is explained by a combination of a) solubility-controlled gas loss from the water, b) addition of sedimentary noble gases, and c) dissolution of unfractionated excess air as follows:

a) All the non-ASW samples were bubbling gas at their collection implying that high F-values can be accounted for by elemental fractionation during liquid-gas phase partitioning. During solubility-controlled liquid-gas phase partitioning, both closed-system batch fractionation and open-system Rayleigh fractionation (Ballentine et al., 2002) would increase *F(132)* and *F(84)* of residual liquid phase as shown in Fig. 6.
b) Alternatively, the high *F(132)* and *F(84)* of the non-ASW samples could be explained by release of atmosphere-derived xenon and krypton that is adsorbed and trapped in sedimentary rocks (Torgersen and Kennedy, 1999). This contribution would be significant and also account for small ^{40}Ar excess relative to air in the most xenon- and krypton-enriched sample (No. 4), because sedimentary noble gases is enriched in radiogenic ^{40}Ar (Podosek et al., 1980). However, actual contribution of sediment-derived ^{40}Ar in total $^{40}Ar^*$ in the sample is difficult to estimate due to uncertainties in sedimentary $^{4}He/^{40}Ar^*$ ratio ranging from 0.003 to 0.05 (Podosek et al., 1980) and that in degree of preferential leaching of ^{4}He from sediment during noble gas uptake into groundwater which have a potential to elevate $^{4}He/^{40}Ar^*$ ratio by a factor of up to 20 (Ballentine and Burnard, 2002).
c) Furthermore, the *F(20)-F(132)* of non-ASW samples at the high *F(20)* side of the fractionation line require addition of unfractionated "excess air" to the residual water bearing fractionated noble gas elemental ratio due to preceding solubility-controlled liquid-gas phase separation (hatched area in Fig. 6) or to the water involving sedimentary heavy noble gases. This contamination occurs as entrapment and dissolution of gas bubbles with atmospheric gas composition (Heaton and Vogel, 1981). At present, however, further quantitative evaluation is difficult on relative importance of the above processes because the absolute concentration of noble gas in bubble-producing water is unknown.

5. Discussion

5.1. Helium isotopes in and around the monogenetic volcano field

Spatial distribution of high $^{3}He/^{4}He$ ratios are interpreted as indicating presence of juvenile magma presently degassing beneath the high $^{3}He/^{4}He$ area. Although the area of high $^{3}He/^{4}He$ (>7 R_A) ratios overlaps the distribution of monogenetic volcanoes (Fig. 7), the remnant magma is not likely to presently degas significant amount of magmatic noble gas because all the monogenetic volcanoes, except Teisi Knoll, erupted more than a few thousand years ago (Koyama et al., 1995). Given that an old magma reservoir is still degassing, the $^{4}He/^{40}Ar^{*}$ ratio of the residual magma would have elevated several orders of magnitude from the original ratio because helium is more soluble than argon in magma (Yamamoto and Burnard, 2005) and the continuous gas discharge would result in large increase in the He/Ar ratio of the residual magma (Fischer et al., 2009). $^{4}He/^{40}Ar^{*}$ ratio of a juvenile magma in the Izu Peninsula can be inferred from melt inclusion-hosted noble gases in olivine phenocryst of old lavas of the monogenetic volcanoes in the east coast of this region. Shimizu et al. (2006) reported $^{4}He/^{40}Ar^{*}$ ratio of 0.8-1.1 for olivine phenocryst of basaltic lava of Iyu-zan, one of the monogenetic volcanoes. The observed $^{4}He/^{40}Ar^{*}$ ratios of this study are close to or lower than that of the lava, supporting presently degassing of a juvenile magma rather than that of an old magma reservoir.

The observed high maximum value of $^{3}He/^{4}He$ ratio reflects the tectonic settings in and around the Izu Peninsula. The maximum value, approximately 8 R_A, is in the range of the maximum value (around 8 R_A) in arc-related volcanic and geothermal fluids worldwide (Hilton et al., 2002), which is equivalent to the range of $^{3}He/^{4}He$ ratio of MORBs (8±1 R_A). In addition, the maximum value is close to that of helium extracted from olivine phenocryst of the Iyu-zan lava (Shimizu et al., 2006). These

319 suggest that helium in the source mantle of the monogenetic volcanoes beneath the Izu
320 Peninsula is brought to a relatively shallow depth by uprising magma and then migrates
321 without or with a minor dilution by crustal helium. A possible interpretation is that the
322 dilution by crustal fluids here is lower than in subduction-type volcanic fields because
323 magmatic gas can easily uprise through vents and eruptive fissure owing to the
324 extension of the crust. This interpretation is consistent with that at Hakone volcano,
325 which is close to the Izu Peninsula but is located on Japan arc (Fig. 1), the highest
326 $^{3}He/^{4}He$ ratio (7.1 R_A: Sakamoto et al., 1992) is slightly lower than that in the Izu
327 Peninsula, because local crust is thicker at Hakone than in the Izu Peninsula (Asano et
328 al., 1985).
329 The characteristic in the distribution of air-corrected $^{3}He/^{4}He$ ratios in the Izu
330 Peninsula is the broad distribution of high $^{3}He/^{4}He$ ratios. The distribution of high
331 $^{3}He/^{4}He$ ratios is so large as to cover over the distribution of monogenetic volcanoes
332 (Fig. 7). Lower $^{3}He/^{4}He$ ratios distribute around them. This is in contrast to the
333 systematic decrease in $^{3}He/^{4}He$ ratio with the distance from the eruption center observed
334 at stratovolcanoes related to subduction-type volcanism (Sano et al., 1984; Williams et
335 al., 1987; Marty et al., 1989; Sakamoto et al., 1992). The vast and relatively uniform
336 distribution of high $^{3}He/^{4}He$ ratios suggests that the permeability for gas movement in
337 the crust is high in and around the monogenetic volcano field in the Izu Peninsula where
338 numerous vents and eruptive fissure may have been formed by the old magma activities.
339 For quantitative discussion, we compared the groundwater residence time based on a
340 box model by Morikawa et al. (2005) between the Izu Peninsula and Ontake volcano by
341 assuming that all the parameters (flux from magma, flux from crust, parameters of
342 aquifer, etc.) except $^{3}He/^{4}He$ ratios are the same between two areas. The difference in
343 drop of air-corrected value of $^{3}He/^{4}He$ ratio, from ca. 7.9 R_A to ca. 6.0 R_A in the Izu
344 Peninsula and from 6.2 R_A to 1.7 R_A at Ontake volcano after traveling similar distance

345 (~20 km), indicates that the groundwater residence time at Ontake volcano is three
346 times longer compared to that in the Izu Peninsula.
347 Correlation between the $^{3}He/^{4}He$ ratios and the terrestrial heat flow in the Izu
348 Peninsula is not clear in our results, although the correlation between them has been
349 pointed out in other areas (e.g., Sano and Wakita, 1985). Since few data of heat flow are
350 available in the Izu Peninsula, we referred to the geothermal gradient data by Tanaka et
351 al. (2004) in Fig. 8. A high geothermal gradient of over 200 (K/km) is reported at close
352 to samples No. 13 and 14, whereas a low geothermal gradient values of about 20~50
353 (K/km) distribute in the western and the northern part of the Izu Peninsula. It appears
354 that high geothermal gradients roughly correlate with high $^{3}He/^{4}He$ ratios. However, we
355 do not discuss this further because of the scarce geothermal gradient data reported for
356 this area (less than 20 points), and poor spatial distribution of them which does not
357 cover the Izu Peninsula homogeneously.
358
359 *5.2. Relation of magma and crustal activities*
360
361 Among the three pressure sources modeled to explain the crustal deformation
362 (see 2.2 seismic swarm activity), sources A and B are located within the distribution of
363 high $^{3}He/^{4}He$ ratios which supports magma is related to them. Source A is an inflation
364 source beneath the center of domal uplift in the earlier stage of the crustal activity.
365 Hagiwara (1977) proposed increase of gas pressure in magma reservoir because he
366 obtained free-air rate gravity-elevation relation. After then the center of uplift shifted to
367 the east coast. Part of the observed uplift is explained by tensile faults (source C) but
368 additional inflation source (source B) is required to explain the entire crustal
369 deformation (Tada and Hashimoto, 1991). In Fig. 7, high $^{3}He/^{4}He$ ratios (>7 R_A) are
370 observed around sources A and B. Since high $^{3}He/^{4}He$ ratios indicate presence of
371 juvenile magma presently degassing as discussed above, the present observation is

372 consistent with existence of magma reservoirs in the vicinity of sources A and B. These
373 magma reservoirs may be constituents of the sporadic magma reservoirs inferred by
374 Koyama and Umino (1991). They inferred that small magma reservoirs distribute
375 sporadically near the upper/lower crust boundary 12-15 km below the monogenetic
376 volcano field by combing petrological, geological and geophysical studies.
377 In contrast, the distribution of $^{3}He/^{4}He$ ratios does not evidently indicate
378 magma in and right below source C1. In Fig. 7, the $^{3}He/^{4}He$ ratios are low at the north
379 side of C1 (samples No. 2 to 5) in contrast to the high $^{3}He/^{4}He$ ratios at the south side
380 (samples No. 6 to 8). High $^{3}He/^{4}He$ ratios are expected to surround C1 if a significant
381 amount of magma with high $^{3}He/^{4}He$ ratio exists below C1 from which magma
382 migrated to the surface through the nearly vertical tensile fault. In this discussion, we
383 assumed high $^{3}He/^{4}He$ ratio (>7 R_A) of the related magma because we do not have any
384 specific reason to assume magma with low $^{3}He/^{4}He$ ratio (<7 R_A) only to the vicinity of
385 C1 in this monogenetic volcano field where high $^{3}He/^{4}He$ ratios are observed almost
386 everywhere. In addition, even if significant amount of magma with low $^{3}He/^{4}He$ ratio
387 (~6 R_A) exists below C1 due to dilution by crustal fluid, the high $^{3}He/^{4}He$ ratios at the
388 south side would not be explained.
389 Alternatively, the distribution of $^{3}He/^{4}He$ ratios suggests magma below a point
390 several kilometers south of C1 instead of right below C1. A possible location of the
391 magma is the area of thermal demagnetization inferred by Sasai and Ishikawa (1991) in
392 the eastern part of the Izu Peninsula (Fig. 7) that explained the large geomagnetic
393 change in 1984-1986. Since this area is surrounded by high $^{3}He/^{4}He$ ratios, our result is
394 consistent with magma in this area. Given that a magma reservoir is located below this
395 area, how the magma causes the seismic swarms; intrusion of magma or fluid
396 pressurization heated by magma? Since our observations may not have spatial
397 resolution to distinguish if magma intruded into C1, both hypotheses remain. On the
398 one hand, the seismic swarms around C1 are consistent with the fluid pressurization of

399 thermal water heated by magma reservoir located apart from C1. On the other hand,
400 magma must move obliquely from the magma reservoir to intrude into C1. Oblique
401 movement of magma during seismic swarms was not plausible because all the tensile
402 faults were modeled almost vertical on the basis of geodetic and seismic data (e.g.,
403 Okada and Yamamoto, 1991; Tada and Hashimoto, 1991). However, Murase et al.
404 (2010) reported that geodetic data in inter-swarm periods is explained with oblique
405 transport of magma from deep reservoir to shallow tensile faults. Their magma reservoir,
406 located close to ours, is consistent with the distribution of $^{3}He/^{4}He$ ratios.
407
408 **6. Concluding remarks**
409
410 (1) Noble gas abundances and isotopic compositions of 31 gas and/or water
411 samples were determined to explore the relation of magma and crustal activity in the Izu
412 Peninsula.
413 (2) $^{3}He/^{4}He$ and $^{4}He/^{40}Ar^{*}$ ratios similar to those of mantle-derived noble gases
414 indicate most of the helium and $^{40}Ar^{*}$ are magmatic origin with a minor contribution of
415 crustal component. Noble gas elemental ratios and neon and argon isotope ratios are
416 basically consistent with their atmospheric origin dissolved in groundwater. Enrichment
417 in heavy noble gases compared to air-saturated water is explained by a combination of
418 solubility-controlled gas loss from the water, addition of sedimentary noble gases, and
419 dissolution of unfractionated excess air.
420 (3) High $^{3}He/^{4}He$ ratio covers a large area over the distribution of monogenetic
421 volcanoes in contrast to the systematic decrease in $^{3}He/^{4}He$ ratio with distance from the
422 eruption center at stratovolcanoes.
423 (4) Among the three pressure sources assumed to explain the crustal
424 deformation, high $^{3}He/^{4}He$ ratios (>7 R_A) distribute around the source A below inland

425 of northeast and source B below the mid east coast, which supports relation of magma
426 with the large crustal uplift observed in the eastern part of the Izu Peninsula.
427 (5) The $^{3}He/^{4}He$ ratios are low (high) at the north (south) side of the tensile
428 fault C1 in the seismic swarm area. The result is not explained if we simply assume
429 magma below C1. Alternatively, the distribution of $^{3}He/^{4}He$ ratios suggests magma
430 below a point several kilometers south of C1. In this interpretation, the seismic swarms
431 are explained to be caused by fluid pressurization of thermal water heated by magma.
432 Another possibility is oblique movement of magma from the deep magma reservoir to
433 shallow tensile faults C1 as Murase et al. (2010) suggested, in which dyke intrusion is
434 the cause of seismic swarms. Although, at present, our result cannot discriminate
435 between dikes and thermal water as the cause of the seismic swarms, our result,
436 independent of geophysical observations, provides valuable information in future
437 investigation of the nature of the crustal activity in the Izu Peninsula.
438
439 **Acknowledgments**
440
441 We are greatly indebted to owners of the wells and town offices who supported our
442 sampling. We thank J.-I. Ishibashi, Y. Shimoike, and A. Shimizu for assistance in
443 sampling and analysis. We make a grateful acknowledgement for comments by T.
444 Fisher, an anonymous reviewer, and the editor that substantially improved this
445 manuscript.
446
447 **References**
448 Aka, F. T., Kusakabe, M., Nagao, K., Tanyileke, G., 2001. Noble gas isotopic
449 compositions and water chemistry of soda springs from the islands of Bioko, Sao
450 Tome and Annobon, along with Cameroon Volcanic Line, West Africa. Appl.
451 Geochem. 16, 323-338.

452 Asano, S., Wada, K., Yoshii, T., Hayakawa, M., Misawa, Y., Moriya, T., Kanazawa, T.,
453 Murakami, H., Suzuki F., Kubota, R., Suyehiro, K., 1985. Crustal structure in the
454 northern part of the Philippine Sea plate as derived from seismic observations of
455 Hatoyama-off Izu Peninsula explosions. J. Phys. Earth, 33, 173-189.
456 Ballentine, C.J., Burgess, R., Marty, B., 2002. Tracing fluid origin, transport and
457 interaction in the crust. In: Porcelli, D., Ballentine, C. J., Wieler, R. (Editors), "-
458 Noble gases – in geochemistry and cosmochemistry". Rev. Mineral. Geochem. 47,
459 539-614.
460 Ballentine, C.J., Burnard, P.G., 2002. Production, release and transport of noble gases in
461 the continental crust. In: Porcelli, D., Ballentine, C. J., Wieler, R. (Editors), "- Noble
462 gases – in geochemistry and cosmochemistry". Rev. Mineral. Geochem. 47,
463 481-538.
464 Burnard, P., Graham, D., Turner, G., 1997. Vesicle-specific noble gas analyses of
465 "popping rock": implications for primordial noble gases in Earth. Science 276,
466 568-571.
467 Cervelli, P., Murray M. H., Segall, P., Aoki, Y., Kato, T., 2001, Estimating source
468 parameters from deformation data, with an application to the March 1997
469 earth-quake swarm off the Izu Peninsula, Japan, J. Geophys. Res. *106*,
470 11217-11237.
471 Dogan, T., Sumino, H., Nagao, K., Notsu, K., 2006, Release of mantle helium from
472 forearc region of the Southwest Japan arc. Chem. Geol. 233, 235-248.
473 Fischer, T.P., Burnard, P., Marty, B., Hilton, D.R., Furi, E., Palhol, F., Sharp, Z.D.,
474 Mangasini, F., 2009. Upper-mantle volatile chemistry at Oldoinyo Lengai volcano
475 and the origin of carbonatites. Nature 459, 77-80.
476 Hagiwara, Y., 1977. The Mogi model as a possible cause of the crustal uplift in the
477 eastern part of Izu Peninsula and the related gravity change. Bull. Earthq. Res. Inst.,
478 Univ. Tokyo, 52, 301-309 (in Japanese with English abstract).

479 Hayakawa, Y., Koyama, M., 1992. Eruptive history of the Higashi Izu monogenetic
480 volcano field 1: 0-32 ka. Bull. Volcanol. Soc. Japan 37, 167-181 (in Japanese with
481 English abstract).
482 Heaton, T.H.E., Vogel, J.C., 1981. "Excess air" in groundwater. J. Hydrol. 50, 201-216.
483 Hilton, D. R., Fischer, T. P., Marty, B., 2002. Noble gases and volatile recycling at
484 subduction zones. In: Porcelli, D., Ballentine, C. J., Wieler, R. (Editors), "- Noble
485 gases – in geochemistry and cosmochemistry". Rev. Mineral. Geochem., 47,
486 319-370.
487 Hoke, L., Poreda, R., Reay, A., Weaver, S. D., 2000. The subcontinental mantle beneath
488 southern New Zealand, characterized by helium isotopes in intraplate basalts and
489 gas-rich springs. Geochim. Cosmochim. Acta, 64, 2489-2507.
490 Honkura, Y., Oshiman, N., Nagaya, Y., 1994. An attempt of searching for a change in
491 the distribution of the geomagnetic total intensity over the site of submarine
492 eruption in the northeastern Izu region, central Japan. J. Geomag. Geoelectr., 46,
493 557-567.
494 Japan Meteorological Agency, 1999, Seismic activity in and around the Izu Peninsula,
495 Rep. Cood. Comm. Earthq. Pred. 61, 218-221 (in Japanese).
496 Kato, T., Iidaka, T., Mizoue, M., 1992. The subcrustal discontinuity with a molten
497 material at the east coast off the Izu Peninsula. Bull. Earthq. Res. Inst., 67, 239-264
498 (in Japanese with English abstract).
499 Koyama, M., Umino, S., 1991. Why does the Higashi-Izu monogenetic volcano group
500 exist in the Izu Peninsula? : relationship between late Quaternary volcanism and
501 tectonics on the northern tip of the Izu-Bonin arc. J. Phys. Earth 39, 391-420.
502 Koyama, M., Hayakawa, Y., Arai, F., 1995. Eruptive history of the Higashi-Izu
503 monogenetic volcano field 2: mainly on volcanoes older than 32,000 years ago. Bull.
504 Volcanol. Soc. Japan 40, 191-209, (in Japanese with English abstract).
505 Marty, B., Jambon, A., Sano, Y., 1989. Helium isotopes and CO_2 in volcanic gases of
506 Japan. Chem. Geol. 76, 25-40.

507 Matsuda, J., Matsumoto, T., Sumino, H., Nagao, K., Yamamoto, J., Miura, Y., Kaneoka,
508 I., Takahata, N., Sano, Y., 2002. The $^{3}He/^{4}He$ ratio of the new internal He Standard
509 of Japan (HESJ). Geochem. J., 36, 191-195.
510 Matsumoto, T., Kawabata, T., Matsuda J., Yamamoto K., Miura K., 2003. $^{3}He/^{4}He$
511 ratios in well gases in the Kinki district, SW Japan: surface appearance of
512 slab-derived fluids in a non-volcanic area in Kii Peninsula. Earth Planet. Sci. Lett.,
513 216, 221-230.
514 Mogi, K., 1985, Earthquake prediction Academic Press, Tokyo, pp. 355.
515 Morikawa, K., Kazahaya K., Yasuhara, M., Inamura, A., Nagao K., Sumino H.,
516 Ohwada M., 2005. Estimation of groundwater residence time in a geologically
517 active region by coupling 4He concentration with helium isotopic ratio. Geophys.
518 Res. Lett., 32, L02406, doi:10.1029/2004GL021501.
519 Morita, Y., Nakao, S., Hayashi, Y., 2006. A quantitative approach to the dike intrusion
520 process inferred from a joint analysis of geodetic and seismological data for the
521 1998 earthquake swarm off the east coast of Izu Peninsula, central Japan. J.
522 Geophys. Res., 111, doi:10.1029/2005JB003860.
523 Murase, M., Ito T., Hayashi Y., Sagiya T., Kimata F., Watanabe H. 2010.
524 Spatio-temporal distribution of magma intrusions inducing repeated earthquake
525 swarms off the east coast of the Izu peninsula, central Japan, for 1973-1998. J.
526 Volcanol. Geotherm. Res., 193, 25-36.
527 Nagao, K., Takaoka, N., Matsubayashi, O., 1979. Isotopic anomalies of rare gases in the
528 Nigorikawa geothermal area, Hokkaido, Japan. Earth Planet. Sci. Lett. 44, 82-90.
529 Nier, A. O., 1950. A redetermination of the relative abundances of the isotopes of
530 carbon, nitrogen, oxygen, argon, and potassium. Phys. Rev. 77, 789-793.
531 Okada, Y., Yamamoto, M., 1991. Dyke intrusion model for the 1989 seismovolcanic
532 activity off Ito, central Japan. J. Geophys. Res. 96, 10361-10376.
533 Okada, Y., Yamamoto, E., Ohkubo, T., 2000, Coswarm and preswarm crustal
534 deformation in the eastern Izu Peninsula, central Japan. J. Geophys. Res. 105,
535 681-692.

536 Okubo, S., Hirata, Y., Sawada, M., Nagasawa, K., 1991. Gravity change caused by the
537 1989 earthquake swarm and submarine eruption off Ito. Japan – test on the magma
538 intrusion hypothesis -. J. Phys. Earth 39, 219-230.
539 Ozima, M., Podosek, F. A., 2002. Noble Gas Geochemistry. Cambridge Univ. Press.,
540 286 pp.
541 Perez, N. M., Nakai, S., Wakita, H., Hernandez, P. A., Salazar, J. M., 1996. Herium-3
542 emission in and around Teide volcano, Tenerife, Canary Islands, Spain. Geophys.
543 Res. Lett. 23, 3531-3534.
544 Peeters, F., Beyerle, U., Aeschbach-Hertig, W., Holocher, J., Brennwald, M.S., Kipfer,
545 R., 2002. Improving noble gas based paleoclimate reconstruction and groundwater
546 dating using $^{20}Ne/^{22}Ne$ ratios. Geochim. Cosmochim. Acta 67, 587-600.
547 Podosek, F.A., Honda, M., Ozima, M., 1980. Sedimentary noble gases. Geochim.
548 Cosmochim. Acta 44, 1875-1884.
549 Sakamoto, M., Sano, Y., Wakita, H., 1992. $^{3}He/^{4}He$ ratio distribution in and around the
550 Hakone volcano. Geochem. J. 26, 189-195.
551 Sano, Y., Nakamura, Y., Wakita, H., Urabe, A., Tominaga, T., 1984. Helium-3
552 emission related to volcanic activity. Science 224, 150-151.
553 Sano, Y., Wakita, H., 1985. Geographical distribution of $^{3}He/^{4}He$ ratios in Japan:
554 implications for arc tectonic and incipient magmatism. J. Geophys. Res. 90,
555 8729-8741.
556 Sano Y., Wakita H. 1988. Precise measurement of helium isotopes in terrestrial gases.
557 Bull. Chem. Soc. Jpn. 61, 1153-1157.
558 Sarda, P., Staudacher, T., Allègre C. J., 1988. Neon isotopes in submarine basalts. Earth
559 Planet. Sci. Lett. 91, 73-88.
560 Sasai, Y., Ishikawa, Y., 1991. Tectonomagnetic signals related to the seismo-volcanic
561 activity in the Izu Peninsula. J. Phys. Earth 39, 299-320.
562 Shimizu, A., Sumino, H., Nagao, K., Notsu, K., Mitropoulos, P., 2005. Variation in
563 noble gas samples from the Aegean arc, Greece. J. Volcanol. Geotherm. Res., 140,
564 321-339.

565 Shimizu, A., Sumino, H., Nagao, K., Notsu, K., Hirano, N., Machida, S. Ishii, T., 2006.
566 Involvement of pore water in the Izu-Ogasawara subduction process: Evidence from
567 argon isotope ratio. Eos Trans. AGU, 87(52), Fall Meet. Suppl., Abstract
568 V41B-1719.
569 Sumino, H., Nagao, K., Notsu, K., 2001. Highly sensitive and precise measurement of
570 helium isotopes using a mass spectrometer with double collector system. J. Mass
571 Spectrom. Soc. Jpn. 49, 61-68.
572 Sumino, H., Notsu, K., Nakai, S., Sato, M., Nagao, K., Hosoe, M., Wakita, H., 2004.
573 Noble gas and carbon isotopes of fumarolic gas from Iwojima volcano,
574 Izu-Ogasawara arc, Japan: implications for the origin of unusual arc magmatism.
575 Chem. Geol. 209, 153-173.
576 Tada, T., Hashimoto, M., 1991. Anomalous crustal deformation in the northeastern Izu
577 Peninsula and its tectonic significance – tension crack model -. J. Phys. Earth 39,
578 197-218.
579 Tanaka, A., Yamano, M., Yano, Y., Sasada, M., 2004. Geothermal Gradient and Heat
580 Flow Data in and around Japan. Digital Geoscience Map DGM P-5, Geological
581 Survey of Japan.
582 Tsuneishi, Y., 1991. Continuous monitoring of crustal activity in east Izu Peninsula by
583 automatic electronic distance measurement. J. Phys. Earth 39, 131-140.
584 Torgersen, T., Kennedy, B.M., 1999. Air-Xe enrichments in Elk Hills oil field gases:
585 role of water in migration and storage. Earth Planet. Sci. Lett. 167, 239-253.
586 Ukawa, M., Tsukahara, H., 1996. Earthquake swarms and dike intrusions off the east
587 coast of Izu Peninsula, central Japan, Tectonophysics, 253, 285-303.
588 University of Tokyo, 2000. Vertical movements in the Izu-Peninsula (1980-1999). Rep.
589 Cood. Comm. Earthq. Pred. 63, 208-215 (in Japanese).
590 Williams, S. N., Sano, Y., Wakita, H., 1987. Helium-3 emission from Nevado del Ruiz
591 volcano, Columbia. Geophys. Res. Lett. 14, 1035-1038.

592 Yamamoto, E., Okada, Y., Ohkubo T., 1994. Ground tilt change associated with the
593 swarm activity off the east coast of Izu Peninsula in May - June, 1993. Rep. Cood.
594 Comm. Earthq. Pred. 51, 336-340 (in Japanese).
595 Yamamoto, J., Burnard, P.G., 2005. Solubility controlled noble gas fractionation during
596 magmatic degassing: Implications for noble gas compositions of primary melts of
597 OIB and MORB. Geochim. Cosmochim. Acta 69, 727-734.
598 Yamamoto, T., Soya, T., Suto, S., Uto, K., Takada, A., Sakaguchi, K., Ono, K., 2001.
599 The 1989 submarine eruption off eastern Izu Peninsula, Japan: ejecta and eruption
600 mechanisms, Volcanology, 53, 301-208.
601 Yamamoto, J., Nishimura, K., Sugimoto, T., Takemura, K., Takahata, N., Sano, Y.,
602 2009. Diffusive fractionation of noble gases in mantle with magma channels: Origin
603 of low He/Ar in mantle-derived rocks. Earth Planet. Sci. Lett. 280, 167-174.
604 Yoshida, S., Seta, G., Okubo, S., Kobayashi, S., 1999. Absolute gravity change
605 associated with the March 1997 earthquake swarm in the Izu Peninsula. Japan, Earth
606 Planets Space, 51, 3-12.
607
608 ----------

609 Figure Captions
610
611 Fig. 1. Location of the sampling points in the Izu Peninsula (squares). Numbers on the
612 points correspond to sample numbers in Table 1. Solid circles indicate monogenetic
613 volcanoes (Koyama and Umino, 1991) and the hatched area roughly indicates the
614 distribution of epicenters of the seismic swarm activities. Lines in the hatched area
615 denote tensile faults (for details, see text and Fig. 2).
616
617 Fig. 2. Contours indicate crustal vertical movement between 1980 and 1999: thick lines
618 indicate neutral lines and solid and dashed lines indicate uplift and subsidence every 60
619 mm, respectively (University of Tokyo, 2000). A star indicates submarine eruption

(Teisi Knoll) on July 13, 1989. Crosses (A and B) and thick and thin lines (C1 and C2, respectively) are assumed pressure sources to explain the crustal deformation (see text). Dotted gray line encloses area below which molten material was suggested by Kato et al. (1992).

Fig. 3. Plot of $^{3}He/^{4}He$ vs. $^{4}He/^{20}Ne$ ratios for bubbling gas or steam (open circles), water (open squares), and samples with approximately 1:1 gas and water (open triangles) in the Izu Peninsula. The lines represent mixing lines between the air-saturated water (ASW) and end members whose $^{3}He/^{4}He$ ratio are 4, 6, and 8 R_A, respectively, and $^{4}He/^{20}Ne$ ratios are 10000. A thick line indicates the variation of $^{4}He/^{20}Ne$ in ASW from 0.268 (20ºC) to 0.335 (100ºC, caluculated after Ballentine et al., 2002).

Fig. 4. Plot of $^{20}Ne/^{22}Ne$ vs. $^{21}Ne/^{22}Ne$ ratios for samples in the Izu Peninsula. A broken line indicates the mass fractionation line of the air component. A mixing line between MORB source mantle and air (MORB line) given by Sarda et al. (1988) is also shown for comparison. Error bars are 1 σ.

Fig. 5. Plot of $^{40}Ar/^{36}Ar$ vs. $^{38}Ar/^{36}Ar$ ratios for samples in the Izu Peninsula. A broken line indicates the mass fractionation line of the air component. Error bars are 1 σ.

Fig. 6. Plot of *F(20)* against *F(132)* for samples in the Izu Peninsula, where F(m) is defined by $F(m) = (^{m}X/^{36}Ar)_{sample}/(^{m}X/^{36}Ar)_{air}$, where ^{m}X stands for ^{84}Kr and ^{132}Xe.. Sample numbers are indicated for selected samples. Endmember compositions of air, air-saturated water (ASW) with temperature range of 20-100ºC (calculated after Ballentine et al., 2002) are also plotted (crosses). Solid and dashed lines show compositional change of residual water originally equilibrated with air at 20 ºC during

647 solubility-controlled batch fractionation and Rayleigh fractionation (Ballentine et al.,
648 2002), respectively. The limits of the fraction of Ar remaining in the water phase and
649 temperature conditions are taken to be 0.01 and 80 ºC. Shaded area indicates a mixing
650 between the residual ASW of solubility-controlled fractionation and unfractionated
651 excess air. Possible addition of heavy noble gases released from sedimentary rocks
652 (Torgersen and Kennedy, 1999) is also indicated by an arrow.
653
654 Fig. 7. Summary of geographical distribution of air-corrected $^{3}He/^{4}He$ ratio in the Izu
655 Peninsula. In the map the $^{3}He/^{4}He$ ratios are indicated by symbols. Shaded area
656 approximates the distribution of monogenetic volcanoes. A dotted circle denotes the
657 periphery of the thermally demagnetized area modeled by Sasai and Ishikawa (1991).
658 Other symbols (star, crosses, and thick and thin lines) are the same as in Figure 2.
659 Numbers indicate the sample numbers of which air-corrected $^{3}He/^{4}He$ ratios are plotted
660 in the right diagram.
661
662 Figure 8. Geothermal gradient (K/km) by Tanaka et al. (2004).
663 **----------**

Table 1

Click here to download Table: Table1revised.doc

Table 1

Type of samples and the feature of wells

No.	Locality	Sample ID	Sampling date	Type[a]	Temperature (℃)	pH	E-Cond[b]. (S/m)
1	Atami	Kasumi	Mar/21/2000	S	...	...	...
2	Ajiro_North	Isofune1	Mar/10/1999	G	82	6.5	3.1
3	Ajiro_South	Isofune2	Mar/10/1999	G	65	6.2	1.7
4	Oishigasawa	Usami35	Mar/10/1999	G	96.2	6.3	2.2
5	Usami	Usami24	May/20/1999	W	63.8	9.3	0.52
6	Ito	Hirono	May/23/2000	G	53.4	8.4	0.13
7	Komuro	Komuro13	Mar/10/2000	W	58	7.6	0.58
8	Ippekiko	Itopia3	May/21/1999	W	40	8.5	0.25
9	Futo_North	Tajima62	Mar/10/2000	W	65	7.9	0.34
10	Futo_South	Sankai	Mar/10/2000	W	46	9.2	0.25
11	Akazawa_North	Akazawa1	Mar/9/2000	G	35.5	8.5	0.048
12	Akazawa_South	Akazawa6	May/21/1999	W	40.9	9.0	0.52
13	Atagawa	Atagawa	Jul/21/1999	S	91.5	7.6	0.46
14	Yugano	Minami	Jul/22/1999	W	42.4	9.1	0.15
15	Rendaiji	Yagohei	Jul/21/1999	G	50	7.6	0.10
16	Shimogamo	Jugei	Nov/16/2001	G	98.3	...	...
17	Kanmnami	Koma	Mar/23/2000	G/W	33.4	9.0	0.025
18	Nagaoka	Kona	Mar/22/2000	G	68.3	8.8	0.10
19	Hiekawa	Gozen	Mar/21/2000	G	54.5	8.1	0.13
20	Shiraiwa	Shiraiwa	Mar/22/2000	G	49	8.7	0.28
21	Otaira	Sparacio	Mar/22/2000	G	50	7.3	0.71
22	Amagi	Amagi	Nov/15/2001	W	43.2	...	...
23	Odoi	Odoi	Mar/23/2000	G	43.3	7.8	0.79
24	Toi	Nakamura	Mar/23/2000	G	55.5	8.1	0.23
25	Neginohata	Negi	Mar/23/2000	G/W	36	9.0	0.18
26	Futoh	Futoh	Mar/23/2000	G	49.6	7.3	1.2
27	Matsuzaki	Sakurada	Nov/15/2001	G	74.6	...	...
28	Nakaizu1	SKE	May/23/2000	W	14.6	7.6	0.015
29	Nakaizu2	RHB	May/23/2000	G	29	7.7	0.021
30	Shuzennji	NewTown	Mar/22/2000	W	21	8.2	0.009
31	Tsukigase	Tsukigase	Mar/21/2000	G	43.3	8.5	0.080

[a] G, gas; W, water; S, steam; G/W partially gas and partially water

[b] Electric Conductivity

Table 2

Click here to download Table: Table2revised.doc

Table 2

Noble gas concentrations and isotopic ratios

No.	^{4}He (ppm)	^{20}Ne (ppm)	^{40}Ar (ppm)	^{84}Kr (ppm)	^{132}Xe (ppm)	^{3}He/^{4}He (R_A)[b]	^{4}He/^{20}Ne	^{3}He/^{4}He cor (R_A)[c]	^{20}Ne/^{22}Ne	^{21}Ne/^{22}Ne	^{38}Ar/^{36}Ar	^{40}Ar/^{36}Ar	^{40}Ar/^{36}Ar f-corrected[d]	^{4}He/^{40}Ar*[e]
1	30	5.0	12000	2.1	0.18	5.43±0.10	6.1	5.68±0.11	9.77±0.02	0.0290±0.0002	0.1886±0.0003	296.3±0.4	294.3±0.4	...
2	25	12	…	...	...	5.56±0.09	2.2	6.35±0.14	...	...	...	...		
3	120	11	...	...	...	5.80±0.12	11	5.95±0.12	...	...	...	...		
4	13	0.80	1400	0.30	0.054	6.80±0.13	16	6.92±0.13	9.80±0.02	0.0291±0.0003	0.1882±0.0003	298.8±0.3	298.1±0.4	1.3
5	32	6.3	...	...	...	5.97±0.10	5.1	6.30±0.11	...	...	...	...		
6	23	13	9700	1.2	0.11	6.22±0.10	1.8	7.38±0.20	9.85±0.01	0.0292±0.0002	0.1877±0.0004	295.9±0.2	296.8±0.3	0.87
7	48	3.4	3100	0.29	0.013	7.35±0.09	14	7.50±0.10	9.78±0.01	0.0290±0.0001	0.1884±0.0006	298.2±0.4	296.9±0.5	4.9
8	24	20	...	...	...	6.12±0.12	1.2	7.89±0.30	...	...	...	...		
9	86	3.2	5000	0.66	0.041	7.16±0.21	27	7.23±0.21	9.75±0.01	0.0289±0.0002	0.1880±0.0005	299.3±0.3	299.3±0.4	1.6
10	19	5.9	11000	1.5	0.091	6.87±0.09	3.2	7.52±0.13	9.71±0.01	0.0289±0.0001	0.1892±0.0004	299.4±0.5	295.6±0.6	...
11	78	19	9800	1.0	0.063	7.66±0.09	4.1	8.22±0.12	9.68±0.02	0.0284±0.0003	0.1873±0.0005	296.1±0.4	298.3±0.5	1.0
12	28	2.3	...	...	...	6.85±0.24	12	7.01±0.25	...	...	...	...		
13	130	4.9	4800	0.57	0.042	7.74±0.04	28	7.82±0.04	9.82±0.02	0.0290±0.0001	0.1892±0.0005	303.1±0.4	299.3±0.5	2.5
14	17	4.7	...	...	...	6.61±0.19	3.5	7.17±0.22	...	...	...	...		
15	20	11	...	...	...	5.41±0.10	1.9	6.30±0.25	...	...	...	...		
16	210	12	17000	1.8	0.12	5.99±0.06	18	6.08±0.07	9.72±0.01	0.0290±0.0001	0.1874±0.0004	297.9±0.5	299.9±0.6	0.94
17	22	16	6800	0.26	0.0039	5.14±0.16	1.4	6.37±0.27	9.82±0.01	0.0290±0.0001	0.1876±0.0003	296.5±0.1	297.8±0.3	0.52
18	120	12	14000	1.8	0.14	6.84±0.14	9.5	7.04±0.15	9.76±0.02	0.0290±0.0002	0.1880±0.0003	297.3±0.4	297.2±0.4	2.1
19	36	12	13000	1.4	0.083	6.98±0.12	2.9	7.71±0.16	9.76±0.02	0.0290±0.0002	0.1884±0.0003	297.1±0.4	295.8±0.5	...

20	140	12	12000	1.3	0.071	6.92±0.12	12	7.09±0.12	9.76±0.02	0.0290±0.0002	0.1880±0.0003	297.8±0.5	297.9±0.5	1.9
21	18	11	8500	1.1	0.069	6.55±0.11	1.6	7.89±0.23	9.76±0.02	0.0291±0.0002	0.1876±0.0004	300.5±0.4	301.7±0.5	0.11
22	6.3	3.1	4700	0.55	0.029	5.54±0.08	2.0	6.38±0.14	9.79±0.01	0.0290±0.0001	0.1875±0.0005	295.5±0.4	297.0±0.5	0.39
23	34	8.9	9600	0.95	0.050	6.14±0.09	3.8	6.60±0.12	9.80±0.04	0.0289±0.0005	0.1883±0.0005	296.3±0.3	295.4±0.4	...
24	16	8.4	12000	1.3	0.078	5.77±0.10	1.9	6.71±0.17	9.78±0.02	0.0291±0.0003	0.1878±0.0004	297.3±0.4	297.9±0.4	0.21
25	29	20	7400	0.31	0.0047	5.80±0.15	1.4	7.16±0.27	9.80±0.01	0.0288±0.0004	0.1871±0.0003	296.9±0.2	299.9±0.3	0.29
26	14	9.5	12000	1.2	0.067	2.97±0.06	1.4	3.54±0.11	9.79±0.02	0.0291±0.0003	0.1879±0.0004	295.4±0.1	295.7±0.3	...
27	41	12	14000	1.4	0.086	6.23±0.06	3.5	6.74±0.09	9.75±0.01	0.0289±0.0001	0.1877±0.0006	296.6±0.3	297.5±0.5	0.58
28	1.1	3.9	7000	1.2	0.12	1.26±0.03	0.28	...	9.81±0.01	0.0292±0.0002	0.1882±0.0004	296.8±0.2	296.1±0.3	0.61
29	4.7	15	8500	0.97	0.096	1.21±0.03	0.312	...	9.92±0.02	0.0294±0.0002	0.1882±0.0003	297.1±0.3	296.6±0.3	0.30
30	1.5	78	7100	0.42	0.0076	1.08±0.06	0.20	...	9.73±0.01	0.0287±0.0001	0.1876±0.0003	297.0±0.1	298.4±0.2	0.03
31	4.4	16	8400	0.76	0.041	1.21±0.08	0.27	...	9.73±0.02	0.0290±0.0002	0.1881±0.0003	297.3±0.5	296.9±0.5	0.17
Atmosphere[a]	5.24	16.45	9320	0.65	0.023	1.00	0.318		9.80	0.0290	0.1880	296.0 [f]		

Errors on abundance are about 10%. Errors with isotopic ratios are 1σ.

[a] Ozima and Podosek (2002).

[b] Normalized to the atmospheric $^{3}He/^{4}He$ ratio=$1.4x10^{-6}$ (Ozima and Podosek, 2002)

[c] Air-corrected $^{3}He/^{4}He$ ratio using $(^{4}He/^{20}Ne)_{air}$=0.318.

[d] Corrected for mass-dependent fractionation based on $^{38}Ar/^{36}Ar$ ratio.

[e] $^{40}Ar^{*}$ denotes non-atmospheric (radiogenic), where $^{40}Ar^{*} = [(^{40}Ar/^{36}Ar)_{sample,f\text{-}corrected}-(^{40}Ar/^{36}Ar)_{air}] \times {}^{36}Ar$.

[f] Nier (1950).

Figure 1

Click here to download Figure: Fig1.pdf

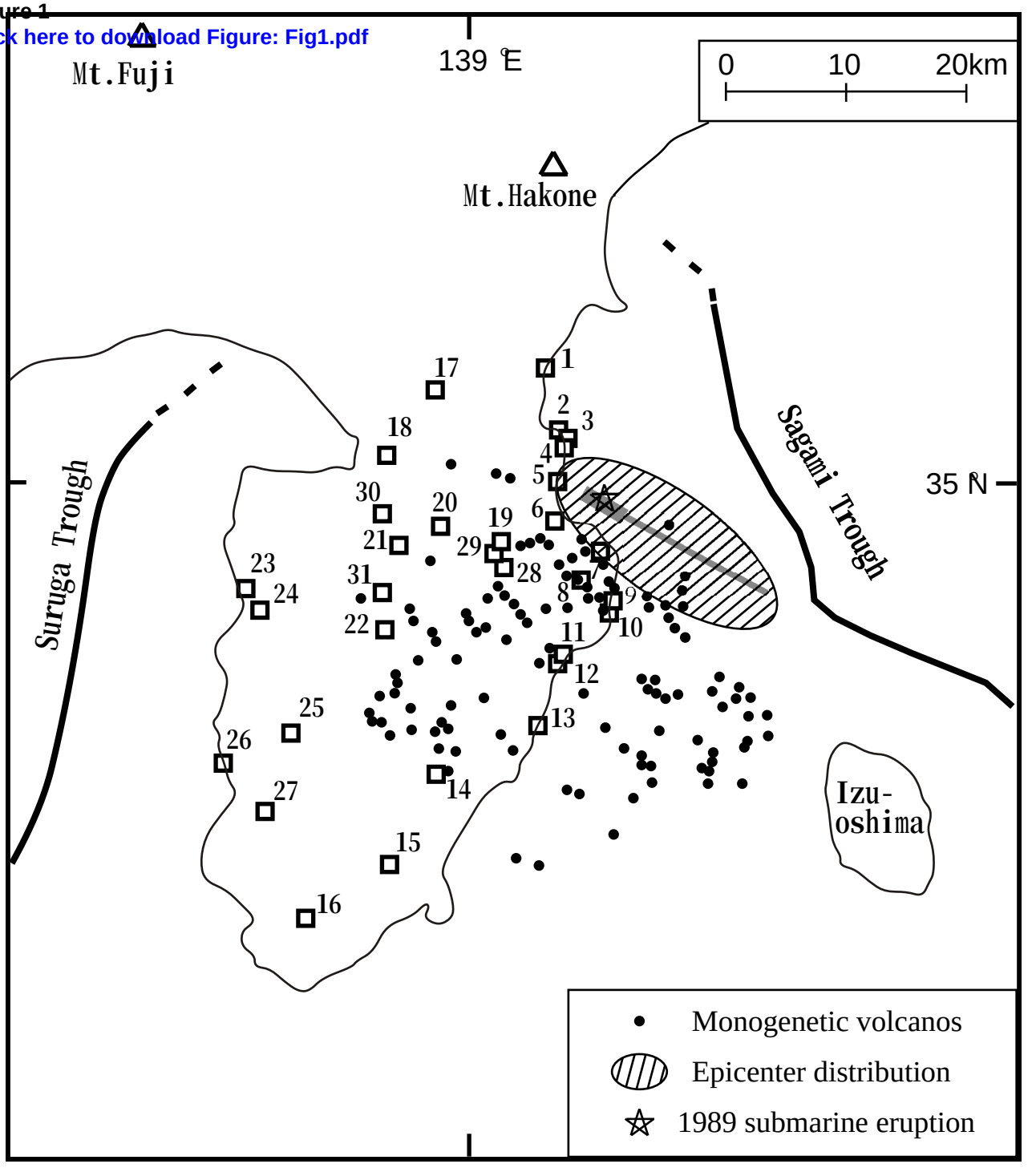

Figure 2
Click here to download Figure: Fig2w.eps

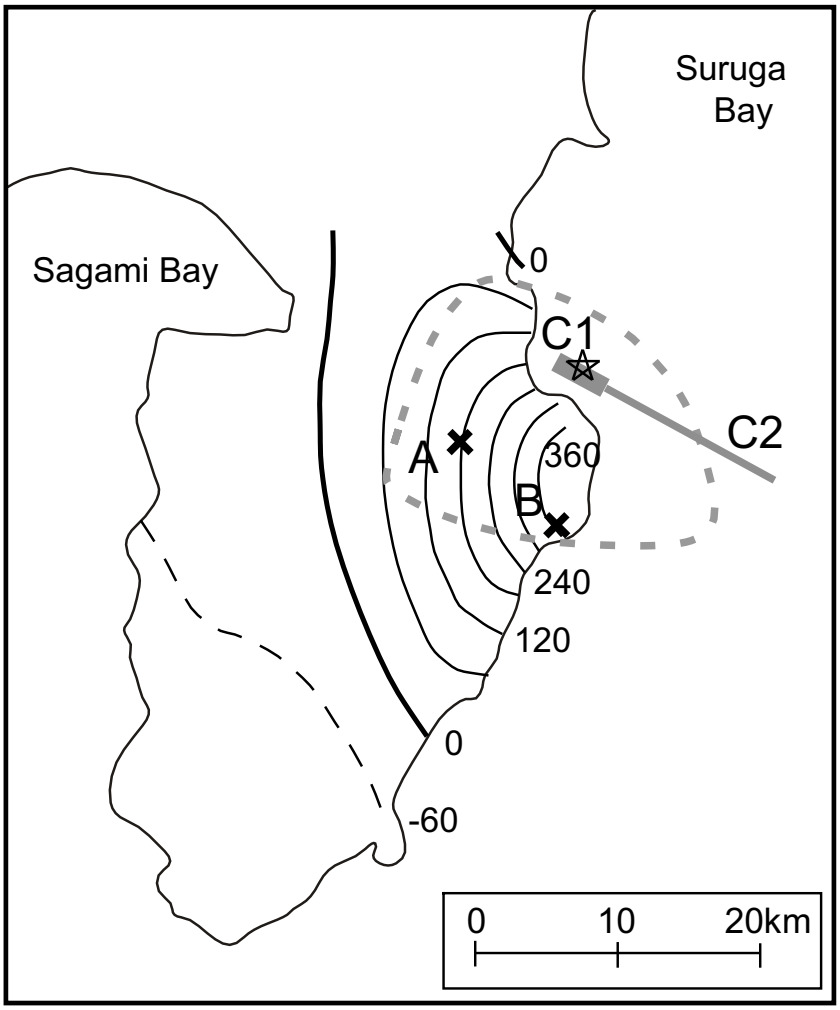

Figure 2

Figure 2

Figure 3
Click here to download Figure: Fig3jugei.eps

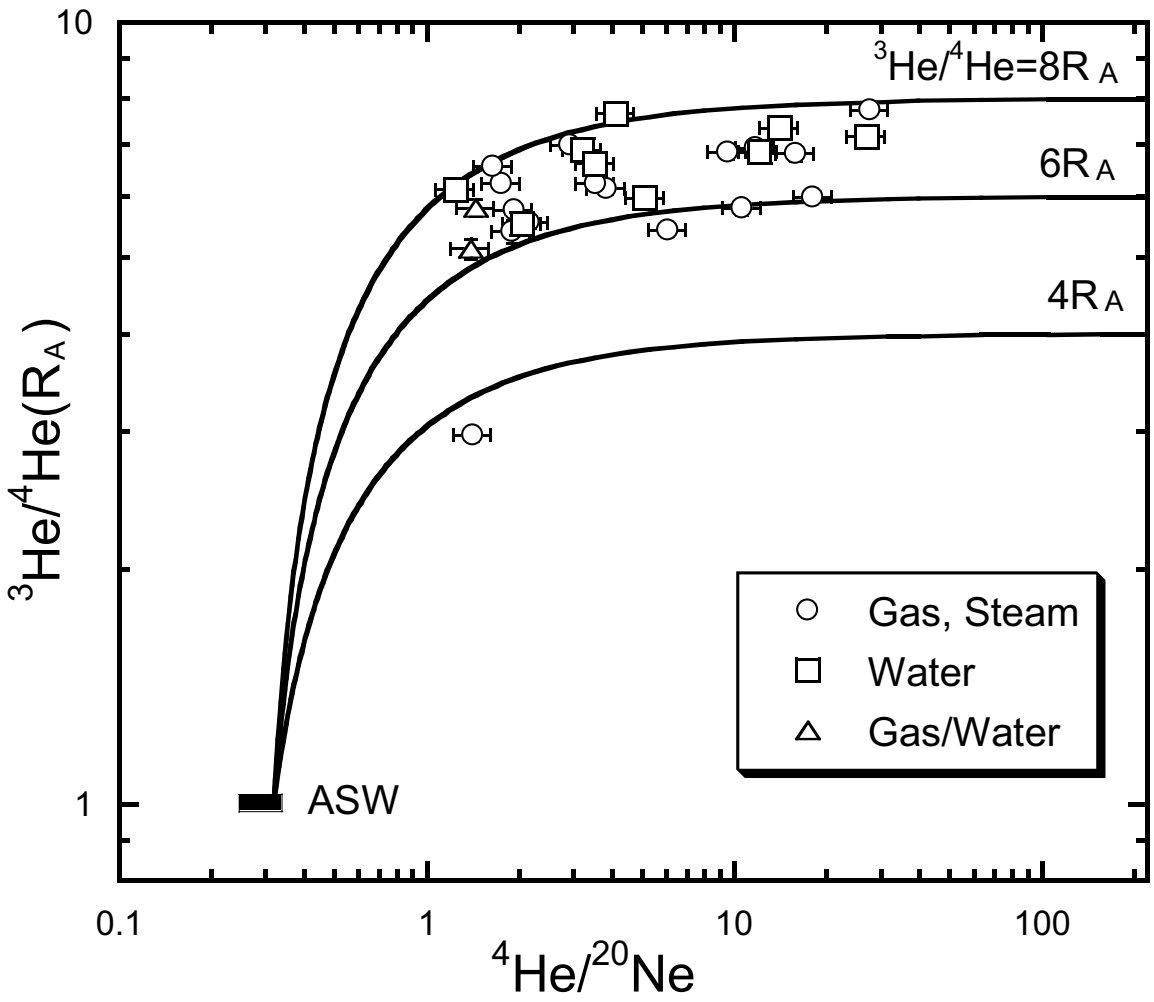

Figure 3

Figure 3

Figure 4
Click here to download Figure: Fig4jugei.eps

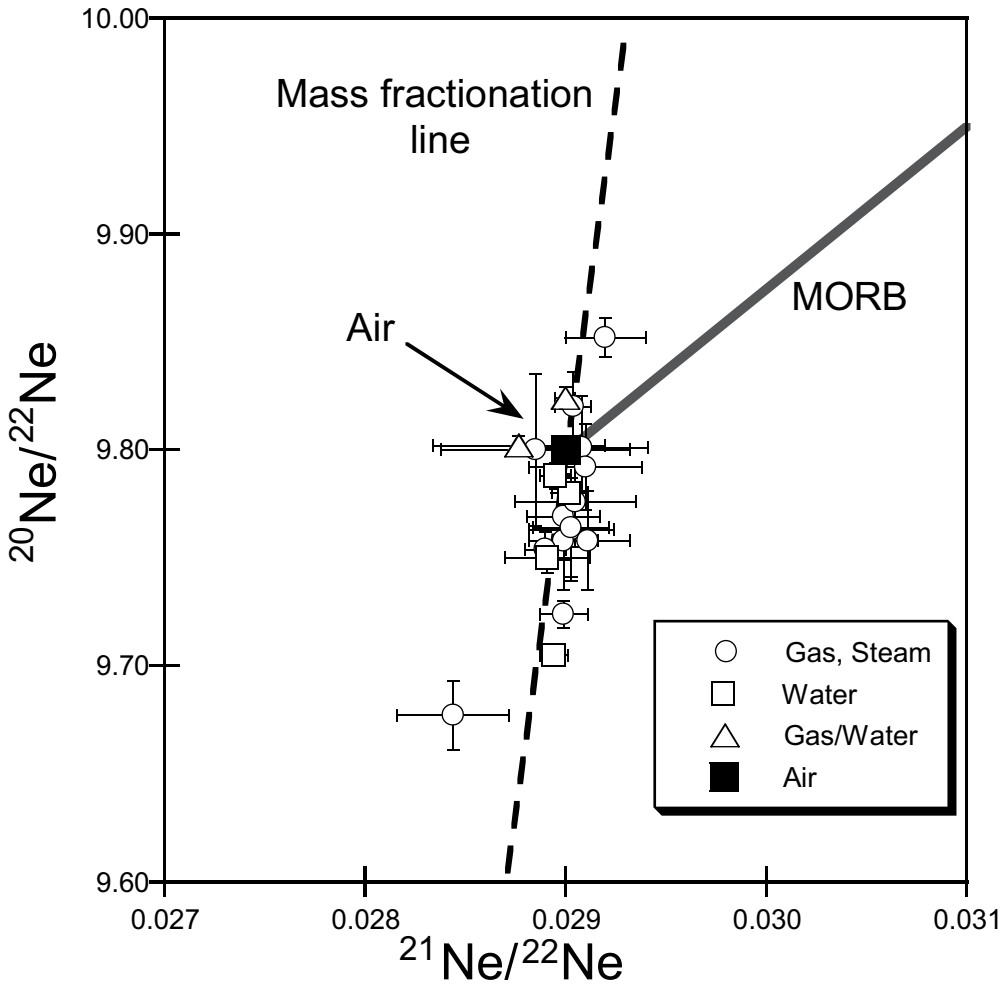

Figure 4

Figure 4

Figure 5
Click here to download Figure: Fig5jugei.eps

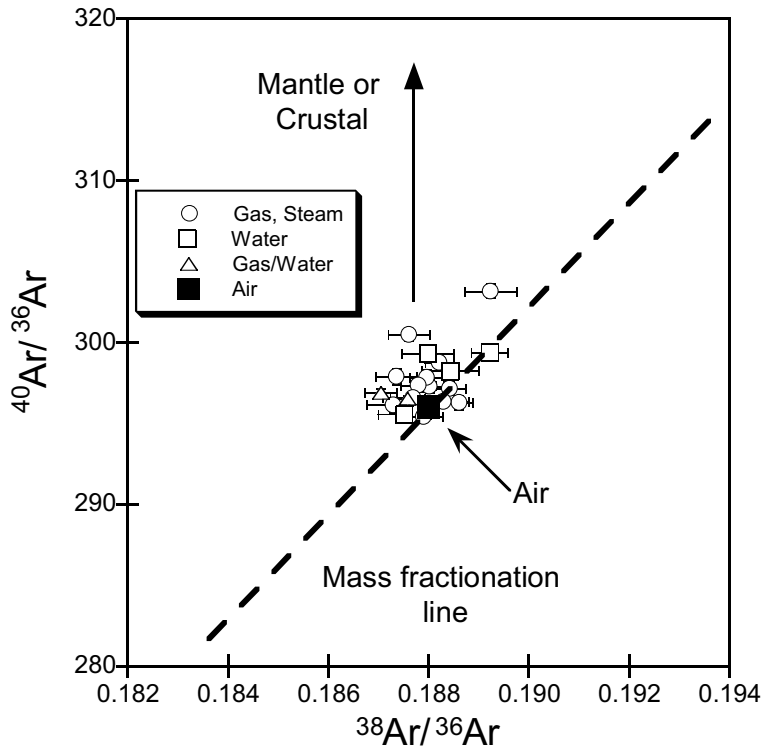

Figure 5

Figure 5

Figure 6
Click here to download Figure: Fig6jugei.eps

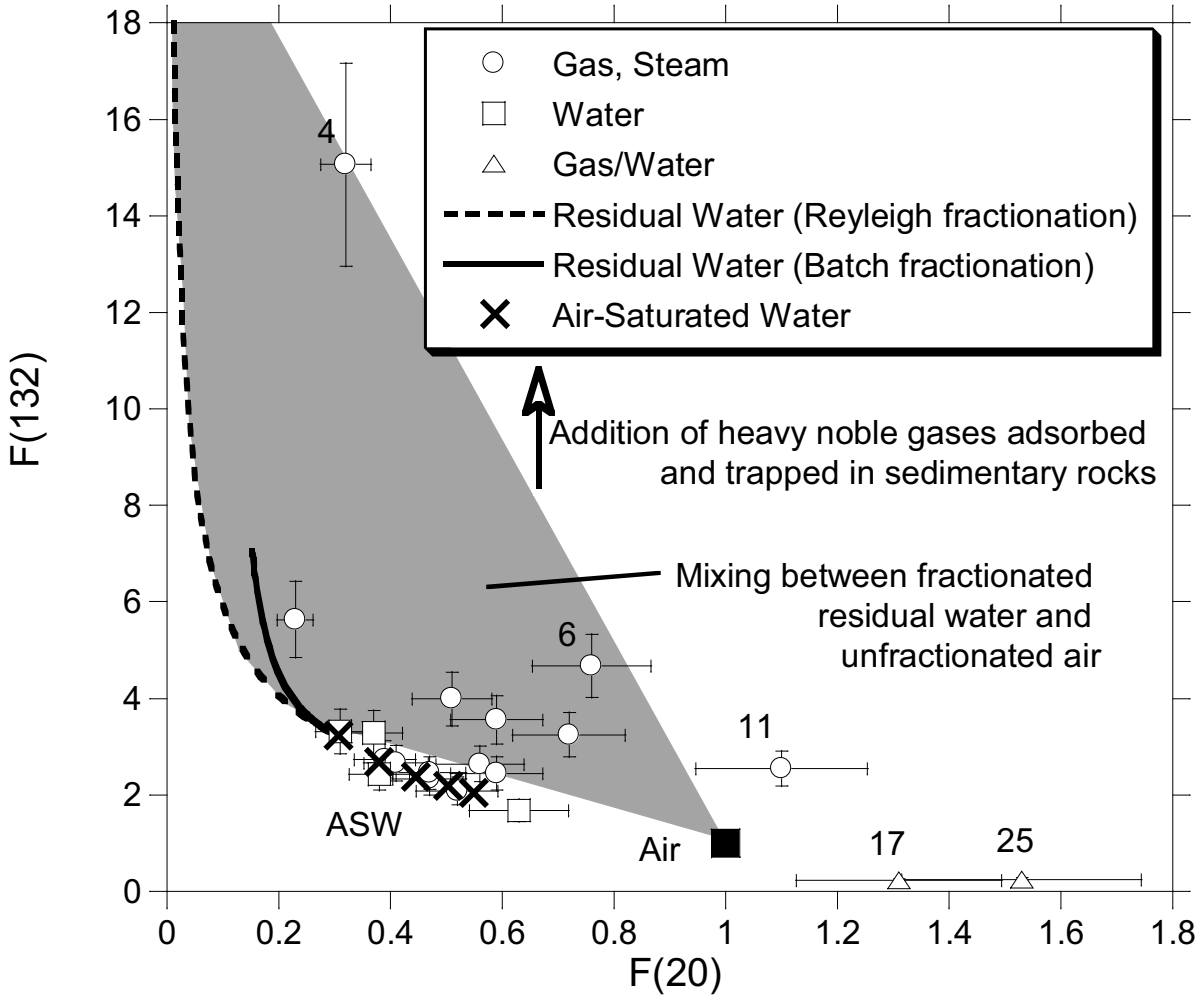

Figure 6

Figure 6

Figure 7
Click here to download Figure: Fig7r.eps

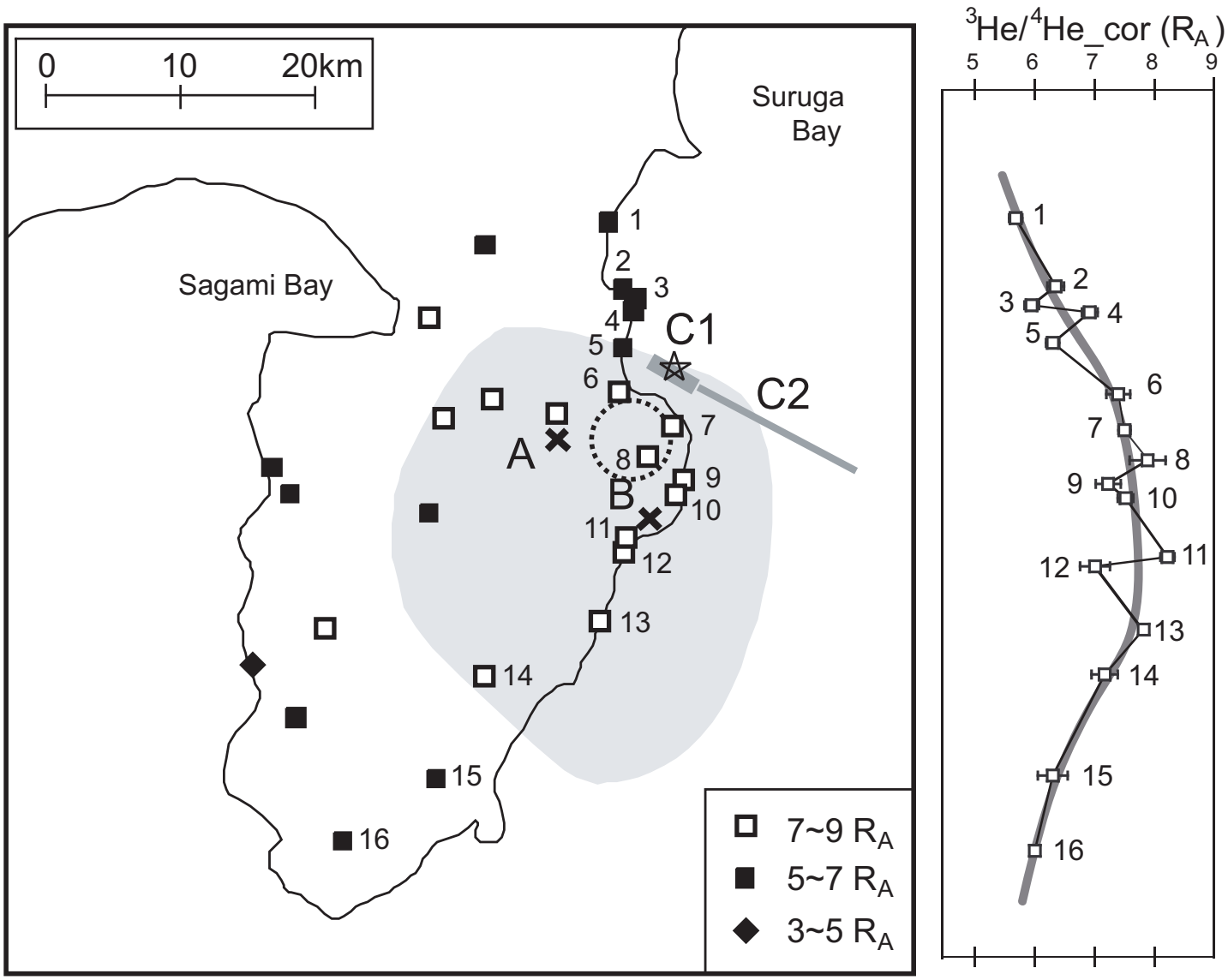

Figure 7

Figure 7

Figure 8
Click here to download Figure: Fig8r.eps

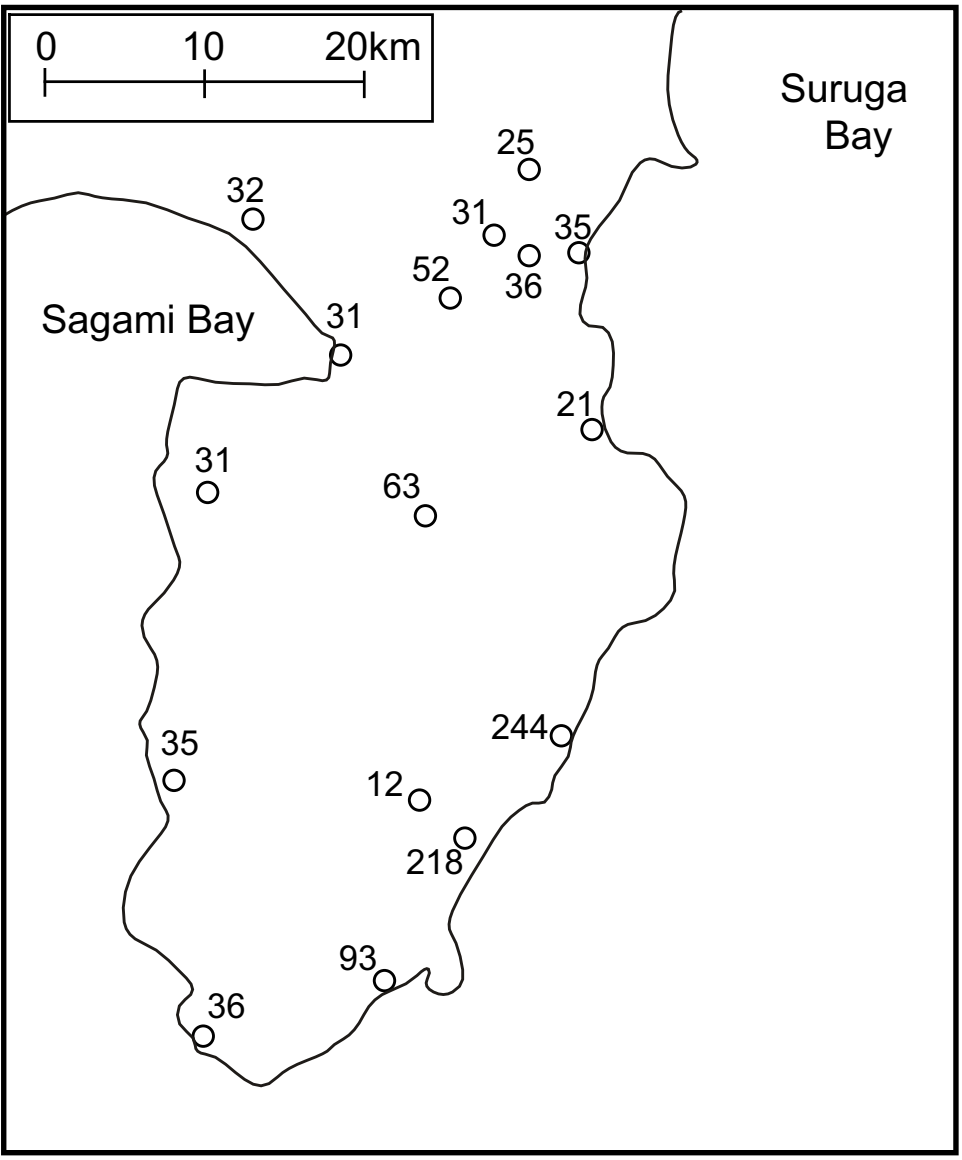

Figure 8